Microbial consortia in salt marsh sediments are sequentially buried over millennia and genomic complementarity analysis indicates an important role in complex carbon decomposition

Joseph H. Vineis[1,2], Ashley N. Bulseco[1,3], Zoe G. Cardon[2], and Jennifer L. Bowen[1]

[1]Marine Science Center, Northeastern University, Nahant, Massachusetts, USA

[2]The Ecosystems Center, Marine Biological Laboratory, Woods Hole, Massachusetts, USA

[3]Department of Biological Sciences, University of New Hampshire, Durham, New Hampshire, USA

Abstract

Salt marsh sediments contain high levels of microbial diversity and functions that reflect the heterogeneity of available nutrients, dynamic hydrology, and layers of organic matter developed over millennia. However, the microbially mediated processes involved in the cycling of complex carbon are still largely undescribed. We used genome reconstruction, co-occurrence networks, and genome scale metabolic modeling to identify the functional capacity for organic matter decomposition and transformation among groups of co-occurring microbes from 5-240 cm of sediment in a *Spartina patens* salt marsh, representing over 3000 years of sediment accumulation. We identified four consortia with similar taxonomic and functional profiles, but distinctly different distributions within the sedimentary layers. Microbial members common to each of these consortia included novel members of Bathyarchaeia BA1, Desulfatiglandales, Chloroflexota, Caldatribacteriota (JS1), Planctomycetota, and WOR3. The collective metabolic potential of these core consortia contained the capacity to decompose complex carbon and aromatics through syntrophic interactions. The composition and

functional potential of these co-occurring members are most similar to communities inhabiting sediment hundreds of meters beneath the surface of deep-sea sediments. Our results suggest that the assembly of communities within the salt marsh sediment are similarly governed by burial and nutrient limitation. The burial processes and putative syntrophy identified here provide a mechanistic understanding of how microbial life can persist under energy limited conditions and contribute to the transformation of carbon within salt marsh sediment.

Keywords: *Spartina alterniflora*, salt marsh sediment, syntrophy, consortia, acetogens, aromatic carbon, Wood-Ljungdahl, benzoyl-CoA

Introduction

Salt marshes are globally important to carbon storage and have the potential to influence both the changing climate and the stability of coastal systems. Salt marsh sediments contain between 400 – 6500 Tg of organic carbon (Duarte et al. 2013; Mcleod et al. 2011) and store an additional 10.2 - 44.6 Mt annually, the equivalent of 0.5-1.0% of anthropogenic C emissions (Ouyang and Lee 2014). However, carbon storage in salt marshes is declining and estimates indicate that over a recent nine-year period, salt marsh habitat loss resulted in emission of 16.3 Tg of CO_2 and a reduction of 0.045 Tg of CO_2 burial per year (Campbell et al. 2022).

Rapidly increasing sea level rise and warming climate could destabilize current stocks of organic carbon with unpredictable consequences (Fontaine et al. 2007; Spivak et al. 2019). Microbial communities within salt marsh sediments are compositionally and metabolically diverse and their interactions influence pools of soil organic carbon (SOC)

(Bulseco et al. 2019; Erb et al. 2024). However, there are important knowledge gaps in our understanding of the metabolic capacity and distribution of microbial communities in 2this system often lead to the identification of previously unidentified carbon cycling among novel taxa (Payne et al. 2025; Seitz et al. 2016; Vineis et al. 2023). Identifying how the pools of carbon are influenced by microbial communities will enhance our understanding of the fate of blue carbon stocks, how they are formed, and how they change over time.

The decomposition of organic material is strongly influenced by plant communities that blanket the surface of the marsh in nearly homogenous stands. The regions of the marsh inhabited by plants are highly dynamic zones that contain hot spots of microbial activity due to plant-microbial interactions and feedbacks that are sensitive to seasonal and tidal influence (Kuzyakov and Blagodatskaya 2015). *Spartina patens* is a highly productive salt marsh macrophyte with roots that release organic carbon and aerate the sediment, thereby influencing carbon sequestration of salt marshes through the “microbial carbon pump” (Liang et al. 2017; Spivak et al. 2019). Live roots of *S. patens* are dominantly 0-10cm below the sediment surface (Gallagher and Plumley 1979) and plant inputs could influence the SOC pool up to 100 cm (Liu et al. 2017).

The patchy distribution of resources and dynamic processes in marsh sediments present challenges for unraveling the underlying rules for community assembly and metabolism. Identifying the distribution and putative functions of the microbial genomes within the dynamic zone influenced by plants and tidal inputs remains one of the most challenging but critical aspects to understanding the carbon and nutrient cycling in salt

marsh systems. While decomposition within the salt marsh is conducted primarily by sulfate reducers (Howes et al. 1984), most of the alternative pathways for anaerobic respiration, fermentation, and carbon fixation pathways have also been identified in marsh sediments (Baker et al. 2015; Vineis et al. 2023; Bulseco et al. 2020) and we are only beginning to understand how many of the carbon cycling processes are linked among organisms and within individual genomes.

Below the rooting zone and beyond the influence of living plants, salt marshes have accumulated vast stores of organic peat that date back, in some cases, millennia (Kirwan et al. 2023). These older sediments are likely to contain microbes adapted to survive in the deep, low energy environment where prior oxidation of organic material has led to a decline in the bioavailability of organic carbon with sediment age and depth (Arndt et al. 2013). Microbial communities below the influence of living plants therefore might mirror other marine low energy sediment communities supported by complex organic matter derived from compounds such as lignin, cellulose, and phenolic polymers (Jørgensen and Boetius 2007). Decomposition of these compounds within energy limited sediment is often dependent on syntrophic interactions among microbial consortia (Peng et al. 2023) The specific mechanism of microbial decomposition has important consequences for carbon stability because microbial turnover can result in the production of carbon that is protected from further decomposition (Liang et al. 2017). Therefore, identifying the capacity for microbial decomposition is important to understanding the susceptibility of long-term carbon storage within salt marsh sediments.

The physical and biogeochemical differences between the dynamic upper layers of the sediment, the energy poor deeper layers, and the transition between the two environments, are likely to support distinctly different microbial communities. We hypothesize that communities within dynamic upper layers will contain genomes with diverse functional potential. Additionally, we hypothesize that the energy limited deeper regions will contain microbial consortia assembled to efficiently metabolize complex carbon. We aim to identify the boundaries of both metabolically flexible genomes and those relying on metabolic handoffs. We also consider the possibility that compositional changes in these low energy sediments will mirror the burial processes observed in marine environments that contain similar energetic limitations (Kirkpatrick et al. 2019; Walsh et al. 2016).

To test these hypotheses, we evaluated the structure and functional potential of microbial communities within 5-240 cm depth fractions from two *S. patens* salt marshes, using a metagenomics and genome reconstruction. Initially, we evaluated the phylogeny, distribution, and co-occurrence of reconstructed draft genomes. We also characterized the potential genomic capacity to decompose organic carbon. Our initial observations of co-occurrence and functional potential prompted us to employ genome-scale metabolic models (GEMs) among co-occurring microbial genomes to identify potential functional complementarity important to carbon cycling.

Methods

1. Sampling

Six sediment cores were taken using a Russian peat corer from the salt marsh platform at two sites in Rowley MA, USA (42.759 N, 70.891 W) primarily vegetated by *Spartina patens*. The sites are part of the Plum Island Ecosystem (PIE) Long-Term Ecological Research site (LTER). Three cores were collected from the high marsh *Spartina patens* platform at two adjacent creeks, West and Sweeney Creek (Fig. 1A). The two creeks are approximately 2 km apart and cores collected within each creek were separated by less than 50 meters. Cores were sampled up to the point of resistance, reaching a maximum depth of 240 cm. Once extracted, subsections of the core were collected approximately every 10 cm and a 2 cm sub-section was homogenized in a sterile 50 mL falcon tube, flash frozen using liquid nitrogen and then stored at -80°C for nucleic acid analysis. A detailed description of sample handling and analysis, including biogeochemistry of the cores has been previously described (Bulseco 2018).

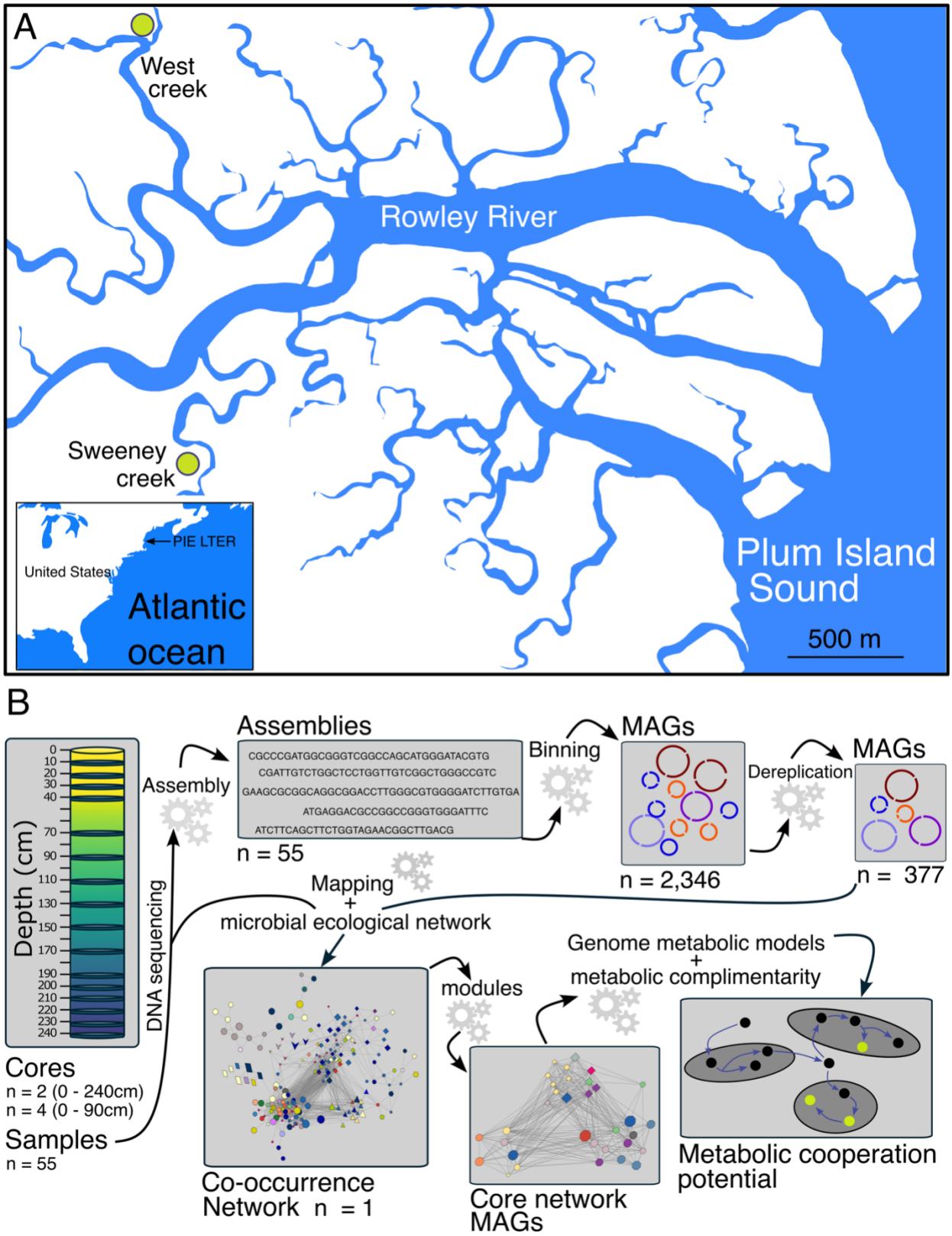
A
West creek
Rowley River
Sweeney creek
PIE LTER
United States
Atlantic ocean
Plum Island Sound
500 m
B
Depth (cm)
0
10
20
30
40
70
90
110
130
150
170
190
200
210
220
230
240
Cores
n = 2 (0 - 240cm)
n = 4 (0 - 90cm)
Samples
n = 55
DNA sequencing
Assembly
Assemblies
CGCCCGATGGCGGGTCGGCCAGCATGGGATACGTG
CGATTGTCTGGCTCCTGGTTGTCGGCTGGGCCGTC
GAAGCGCGGCAGGCGGACCTTGGGCGTGGGGATCTTGTGA
ATGAGGACGCCGGCCGGGTGGGATTTC
ATCTTCAGCTTCTGGTAGAACGGCTTGACG
n = 55
Binning
MAGs
n = 2,346
Dereplication
MAGs
n = 377
Mapping
+
microbial ecological network
Co-occurrence Network n = 1
modules
Core network MAGs
Genome metabolic models
+
metabolic complimentarity
Metabolic cooperation potential

127

128 Figure 1. A) Map of the coring locations within the Plum Island Estuary Long Term
129 Ecological Research (PIE LTER) site and B) Details of core sampling and the
130 bioinformatic approach used to identify metabolic complementarity among co-occurring
131 MAGs within the sediment layers.

132 **2. Metagenomic Sequencing**

133 The input DNA for sequencing library construction was extracted from homogenized
134 sediment from each 2 cm thick fraction (0.25 g wet weight) using a Qiagen Power Soil
135 DNA extraction kit (Qiagen, Germantown, MD) according to the manufacturer's
136 recommendations. We evaluated the quality and the quantity of DNA using a Nanodrop
137 and Quant-IT DNA assay (Invitrogen, USA) respectively. Purified DNA was shipped
138 overnight to the Joint Genome Institute (JGI) on dry ice. At JGI, libraries were created
139 using paired-end (PE) library construction with an insert size of 250 bp. Each library was
140 uniquely barcoded and sequenced according to PE 2x151 chemistry on an Illumina
141 NovaSeq. Sequences were quality filtered using the default settings of BBTools v38.26
142 at JGI (https://jgi.doe.gov/data-and-tools/bbtools/). Quality filtered sequences of each
143 sample were independently assembled using SPAdes assembler 3.12.0 (Bankevich et
144 al. 2012).

145 **3. MAG reconstruction, dereplication, phylogenomics and metagenomic read**
146 **recruitment**

147 We used assemblies and quality filtered sequences generated by JGI/IMG for each of
148 the 55 samples to reconstruct metagenome-assembled genomes (MAGs) for each
149 independent sample (Fig. 2B). The assembled MAGs represent a population of cells.

150 Therefore, we refer to MAGs as populations or population genomes. Genome
151 reconstruction efforts can be improved by co-assembly of multiple samples in a gradient
152 or time series, especially when read counts are not sufficient to provide the minimum
153 amount of coverage necessary for assembly (Stewart et al. 2018). However, the
154 detection of redundant genome populations across samples requires that genome
155 reconstruction be carried out for each sample independently. Additionally, the number of
156 high-quality genomes recovered can be improved by reconstructing genomes from
157 individual samples compared to co-assembly of multiple samples (Olm et al. 2017).

158 We reconstructed draft genomes for each sample using CONCOCT (Alneberg et
159 al. 2014) as an automated guide for genome binning, followed by manual curation of
160 each CONCOCT MAG in Anvi'o, using contig tetranucleotide frequency, coverage,
161 taxonomic assignment, completion, and contamination to guide this process (Eren et al.
162 2015; 2020). In cases where the placement of contigs could not be resolved among a
163 group of similar MAGs, we used anvi-refine to provide increased resolution on this
164 subset of similar MAGs. This allowed for the separation of closely related MAGs and/or
165 the improvement of draft genome bins, as determined by Anvi'o real-time completion
166 and contamination scores.

167 Dereplication of the MAGs and selection of the representative MAG from the
168 dereplicated collections were conducted using the default settings for dRep (Olm et al.
169 2017). Default settings in dRep include dereplication of genomes with an average
170 nucleotide identity (ANI) of 0.95 and a minimum overlap of 10% between the two
171 genomes. dRep incorporates additional essential methods, including CheckM (Parks et
172 al. 2015) and FastANI (Jain et al. 2018). dRep uses completion and contamination

173 based on checkM, which were never at or above the 75% threshold for any of the
174 Patescibacteria. Patescibacteria MAGs were dereplicated separately without a checkM
175 quality score filter. We used the GTDB-Tk to assign taxonomy to each of the MAGs
176 recovered using default settings (Chaumeil et al. 2020).

177 To identify the phylogenomic relationships among the collection of dereplicated
178 MAGs, we first exported the amino acid sequence of the best hit for 71 single copy
179 genes (Bacteria_71). The amino acid sequences for these genes were aligned using
180 MUSCLE and the alignment was trimmed using trimAL v1.4 (Capella-Gutiérrez et al.
181 2009). We reconstructed the phylogenetic tree using the concatenated sequence
182 alignment according to anvi-gen-phylgenomic-tree which employs the FastTree tree
183 building algorithm (Price et al. 2009). The fasta file of single copy gene sequences,
184 alignment, tree, and additional details of phylogenetic reconstruction are available in this
185 github repository https://github.com/jvineis/DEEP-CORE-MANUSCRIPT.git

186 We mapped the metagenomic reads from each sample to the collection of
187 dereplicated MAGs using bowtie2 v2.5.3 (Langmead and Salzberg 2012). Unmapped
188 reads were filtered from the results and samtools v1.19.2 (Li et al. 2009) was used to
189 tabulate the number of reads recruited to each MAG. The relative abundance of each
190 MAG was estimated by dividing the number of reads mapped to the MAG by the
191 number of reads recruited to the non-redundant collection of MAGs.

192 **4. Identifying co-occurring MAGs using network reconstruction**

193 To identify groups of co-occurring genome populations that may be indicative of a
194 shared niche space and/or burial trajectory, we constructed a molecular ecological

network (MEN) using random matrix theory (RMT) according to the procedures recommended by iNAP (Feng et al. 2022). RMT is more commonly used for functional or phylogenetic marker genes but is broadly designed to identify co-occurrence patterns among complex datasets that contain large numbers of variables (species occurrence, microarray data, marker genes) (Gibson et al. 2013). The count matrix of reads recruited to each of the 377 dereplicated MAGs was used as the input for RMT MEN construction. Following log transformation of the count matrix, an adjacency matrix was calculated according to Pearson correlation coefficients. To separate significant co-occurrence from noise, RMT estimates the nearest neighbor spacing distribution (NNSD) within the entire correlation matrix. A random matrix of NNSD values will follow a Gaussian distribution and a non-random matrix will follow a Poisson distribution (Luo et al. 2007). To identify the threshold where the correlation estimates transition from Gaussian to Poisson, we ran iterations of successively smaller correlations starting at 1 with a step size of 0.01. A Chi-square test was used to evaluate transition from a Poisson to a Gaussian distribution at each step and iNAP created a plot of resulting p-values to evaluate each step. Visual inspection of the cutoff indicated that correlations below 0.92 were more likely due to random noise (Fig. S1). All correlations below this 0.92 cutoff were set to zero and a network was constructed. RMT network properties were calculated for the resulting filtered network, including R-square of the power-law relationship. A network containing few MAGs with large numbers of connections with other MAGs will have connectivity that follows a power-law distribution. If the connectivity doesn’t fit the power-law distribution, this indicates that there are many MAGs with high connectivity to other MAGs (a very dense network). Module separation

218 and identification of module hubs were calculated according to a greedy modularity
219 optimization (Newman 2004). Within-module (Z) and among-module connectivity (P)
220 were used to classify each MAG as a network hub (Z > 2.5 and P > 0.62), module hub
221 (Z > 2.5 and P < 0.62), connector (Z < and P > 0.62), or peripheral (Z < 2.5 and P <
222 0.62) (Deng et al. 2012). Based on previous ecological interpretation of networks, the
223 peripheral, connector hub, module hub, and network hub might represent a continuum
224 from specialist to generalist in that order (Olesen et al. 2006). For our purposes of
225 identifying co-occurring genomes, we focused on the identification of modules, which
226 are interlinked subsets of MAGs, and connector hubs that could be important to the
227 stability of the different modules (Olesen et al. 2006).

228 **5. Metabolic potential and distribution of MAGs within identified network**
229 **modules.**

230 To estimate the differences in functional potential among the RMT modules, we
231 constructed a matrix composed of KEGG functional IDs obtained using anvi-estimate-
232 metabolism. MAGs that were included in modules containing fewer than four members
233 or not assigned to a module were also removed from the matrix. We constructed an
234 Atchinson distance matrix and built an NMDS ordination using the vegdist and
235 metaMDS functions respectively. We tested the influence of RMT module and
236 taxonomic classification at the phylum level on the community turnover using the envfit
237 function. All diversity analysis was conducted in R (Core Team 2024) with functions
238 contained in the vegan package (Oksanen et al. 2024). Relative abundance of MAGs
239 within each module were visually inspected to identify their distribution within the vertical
240 sediment profile.

241 **6. Connector hub (Bathyarchaeia BA1) subnetwork genome scale metabolic**
242 **networks**

243 Visualization of the complete RMT network (described above) using Cytoscape
244 (Shannon et al. 2003) led to the identification of four modules with similar taxonomy,
245 functional profiles, and high relative abundance within deeper sediment layers. The
246 MAGs identified as connector hubs common to all four modules, Bathyarchaeia BA1,
247 was used to identify a subnetwork of MAGs that were positively connected and
248 therefore contained the potential for metabolic complementarity. Focusing on MAGs in
249 this subnetwork, we estimated the metabolic potential for key pathways related to
250 decomposition of organic compounds, aromatics, acetate, hydrogenases, and other
251 pathways important to carbon cycling within low energy sediment environments using
252 METABOLIC according to the default parameters (Zhou et al. 2022). We reconstructed
253 genome-scale metabolic networks (GSMNs) using gapseq (Zimmermann et al. 2021)
254 and miscoto (Frioux et al. 2018) was employed to screen GSMNs for key members of
255 minimal communities required to produce the metabolites of the entire community.
256 Analysis of GSMNs was employed using Metag2Metabo (M2M) (Belcour et al. 2020).
257 This approach identifies putative metabolites produced by the co-occurring members of
258 the network module, the key microbial taxa required to produce these metabolites, and
259 interchangeable (redundant) members of the network module.

260

261 **Results**

262 **1. Diverse MAG populations were broadly distributed within salt marsh**
263 **sedimentary layers and both sites**

264 We generated 645.9 Gbp sequences from 55 samples collected up to ~240 cm of
265 salt marsh sediment from six cores (Fig. 1B). The manual genome binning and
266 refinement effort for each of the 55 samples recovered a total of 2,346 MAGs.
267 Dereplication resulted in a collection of 377 MAGs that included 44 phyla, with novel
268 MAGs identified at the class, family, order and genus level (Table S1). The dereplicated
269 MAGs were an average of 87% of expected single copy genes (completion) and 2.7%
270 of these genes found more than once (contaminated) (Fig. 2, Table S1).

271 Most of the MAGs recovered represented novel families within Bacteria and
272 Archaea and were well distributed within the layers of sediment (Fig. 2) and
273 dereplication revealed that many of the MAGs were independently recovered from
274 multiple metagenomic samples (Fig. 3). Phyla containing the largest number of MAGs
275 included Chloroflexota, Planctomycetota, Alphaproteobacteria, Gammaproteobacteria,
276 and Desulfobacterota. A large fraction of the Chloroflexota MAGs were
277 Dehalococcoidia, which were primarily detected in sediment layers below 70 cm and
278 Anaerolineae which had a shallower distribution (Fig. 2). Nearly all 41 MAGs in the
279 Planctomycetota were primarily located below 40 cm. MAGs classified as
280 Desulfobacterota were primarily found in shallow samples, but a distinct clade was
281 detected primarily within shallow sediment. The 39 Proteobacteria MAGs were split
282 evenly between Alphaproteobacteria with MAGs that span the entire depth of sampling
283 and Gammaproteobacteria that were mostly detected in sediment above 40 cm (Fig. 2).
284 Similarly, the 28 MAGs within the phylum Bacteroidota were partitioned according to

depth, although not as strictly as Alpha and Gammaproteobacteria. Within the Bacteroidota, families Vadin HA17, UBA10428, and UBA5072 were generally found below 30-40 cm while Ignavibacteriaceae were found at 10 cm.

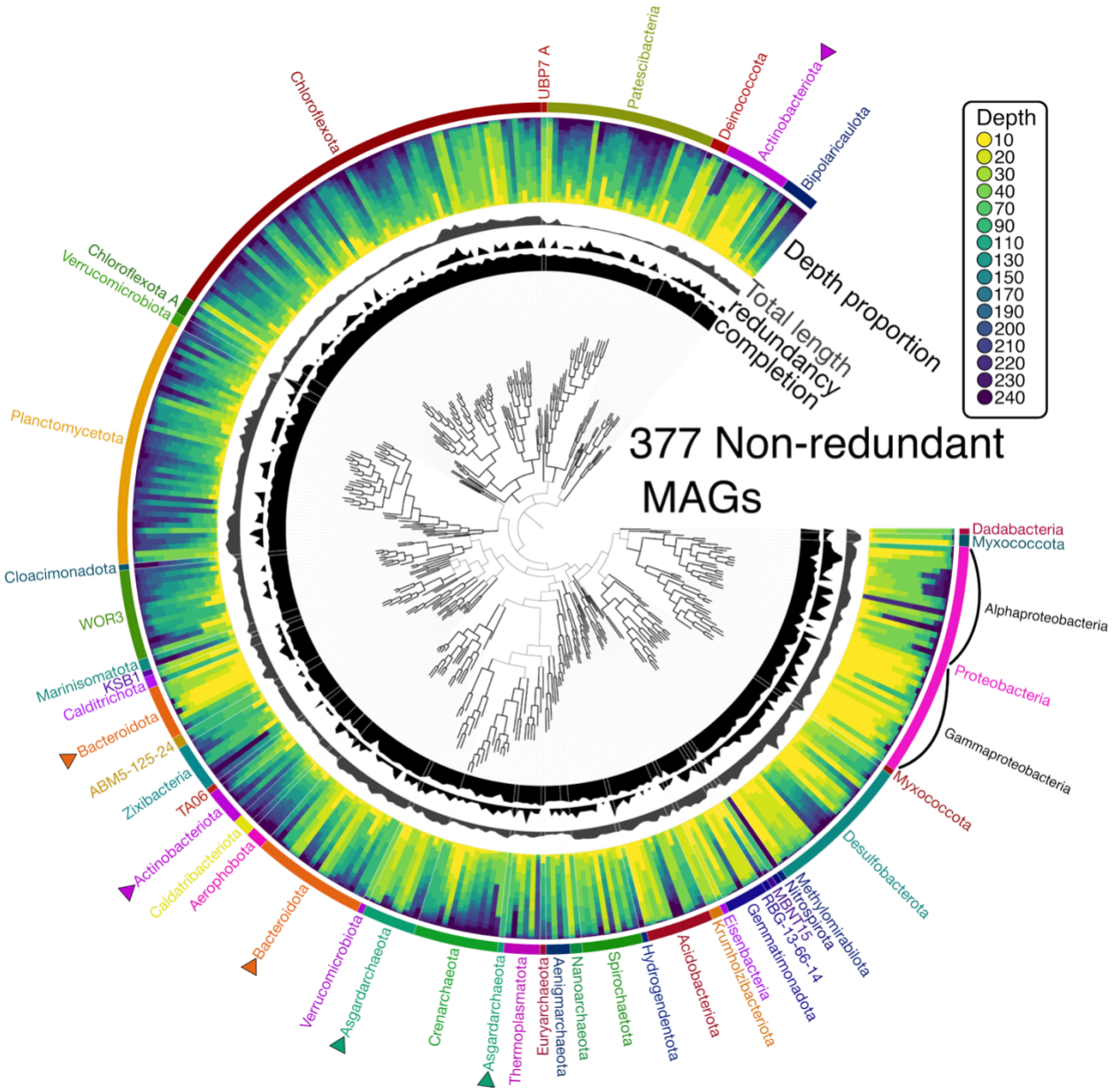

Figure 2. The tree at the center of the display shows the phylogenetic relationship among all MAGs. The innermost ring is a histogram the single copy gene completion estimate (range = 0-100%), followed by redundancy (range = 0-10%), total length of the genome (range = 0-7.6Mbp). The “Depth proportion” ring shows the proportion of the total reads mapped to a MAG from each depth. The outermost ring shows the phylum

level taxonomy as a color bar with matching text. Arrows are positioned adjacent to phyla names with split positions in the tree.

The number of MAGs contained in each dereplicated cluster ranged from 1 to 30 (Fig. 3). Some examples of genome populations represented by a large cluster of dereplicated genomes include 25 independently reconstructed *Ca. Aminicenans* that were reduced to two unique MAGs, 63 Actinobacteriota reduced to 4 MAGs, 52 *Bipolaricaulia* reduced to 6 MAGs, 85 WOR3-B reduced to 11 MAGs, and 24 TA06 reduced to 1 unique MAG (Fig. 3). Many of the MAGs were recovered independently from more than one depth and often from different cores at locations adjacent to different creeks (Fig. 3). In some instances, MAGs from the same dereplicated cluster were independently reconstructed from the top 10-20 cm and below 200 cm. For example, a dereplicated WOR3 MAG contained nearly 30 independently assembled MAGs from samples that spanned the entire 10-240cm vertical profile (Fig. 3). The Desulfobacterota, Bacteroidota, Actinobacteriota, Planctomycetota, and Chloroflexota each contained several MAGs that were recovered from all depths. Sparsely detected Proteobacteria, Gemmatimonadota, and Asgardarchaeota were recovered predominantly from shallow sediment layers, 90cm and above (Fig. 3).

The proportion of metagenomic sequences recruited (mapped) to our collection of nonredundant MAGs was generally greater in sediment samples collected below 40 cm (Fig. S2). Read recruitment below 40 cm was at least 35% and reached nearly 60% in most of the samples below 90 cm. Conversely, metagenomic sequences from sediment samples collected from above 20 cm recruited less than 20% of sequences per sample (Fig. S2) and the number of MAGs recovered was generally lower.

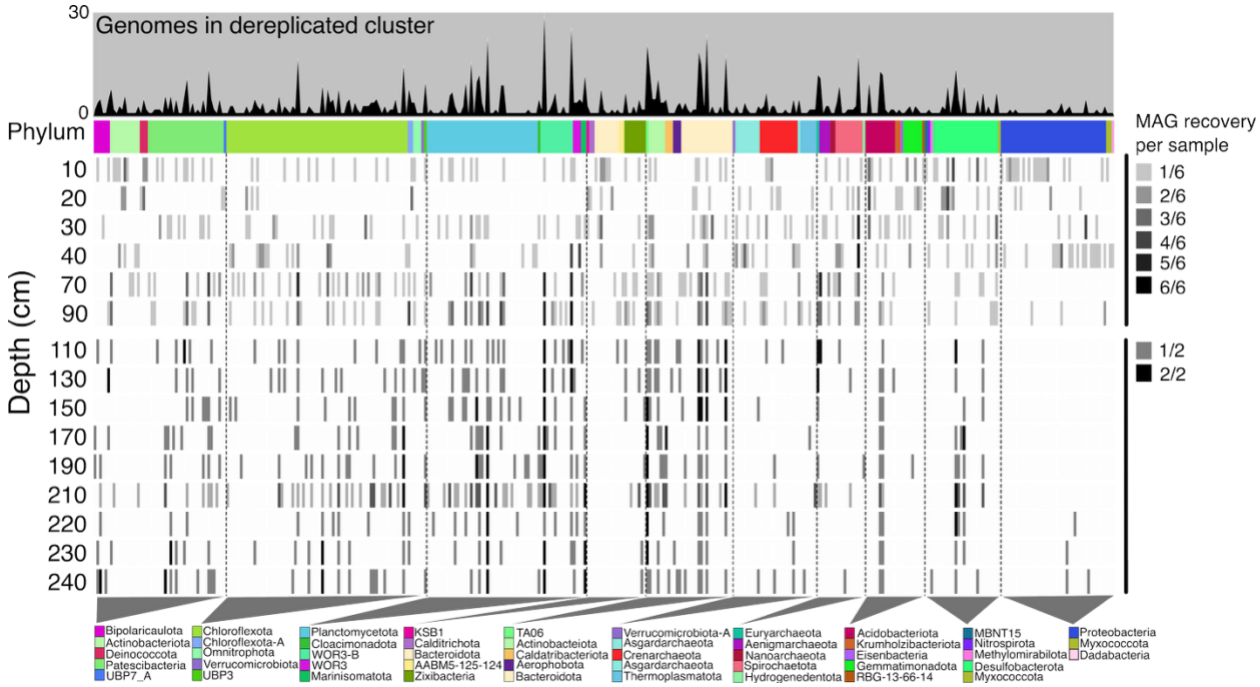

Figure 3. Summary of redundant genome recovery per sample. The line plot at the top of the figure (dark gray and black) shows how many genomes were grouped into the dereplicated genome cluster. The second layer from the top represents the phylum level classification for the representative MAG in the cluster. The heat map layers show the proportion of samples where a MAG in the dereplicated genome cluster was recovered. The key indicating how many of the same MAGs (identified by dRep) were collected per depth is shown on the right. The MAGs are organized according to the phylogenetic reconstruction outlined in the methods section. The phylum color key is shown at the bottom of the figure and the gray triangles above the phylum color align with the heatmap.

2. Co-occurring MAGs

2.1 Strong positive correlations exist among groups of functionally similar MAGs in the deeper sediment layers

Based on MAG relative abundance, we identified a connected network containing 1547 positive connections (edges) among 226 of the 377 MAGs and zero negative

336 edges (Fig. 4A). Most of MAGs were peripheral nodes in the network, but one MAG
337 (Dehalococcoidales – UBA5760) was identified as a module hub and 15 MAGs were
338 classified as connector hubs (Fig. S3). Among the connector hubs were two
339 Bathyarchaeia classified as BA1, two Dehalococcoidales, Desulfatiglandales, and GIF9
340 MAGs. The R^2 of the power-law was 0.97, indicating a scale-free network where most
341 MAGs in the network have few connections. We chose to focus our functional
342 analysis on the top seven modules identified in the network because the remaining 11
343 modules contained fewer than 5 MAGs (Table S1).

344 Modules 1 and 2 contained the largest number of MAGs with a high degree of
345 connectivity within and between the two modules (Fig. 4A). Modules 1 and 2 were also
346 diverse, containing MAGs from 14 and 23 phyla respectively. MAGs within module 7
347 contained many positive links with modules 1 and 2 and the functional potential among
348 MAGs within these three linked modules was very similar (Fig. 4B, Fig. S4). However,
349 modules 1 and 2 contained larger dispersion in the ordination than module 7 due to the
350 presence of Patescibacteria, which were functionally distinct from other MAGs, largely
351 due to their limited functional potential. Most of the Patescibacteria contained fewer than
352 800 genes (Table S1). A relatively large proportion of MAGs in modules 1, 2, and 7 (>
353 25%) contained pathways for complex carbon decomposition, fermentation, amino acid
354 metabolism, and several C1 pathways (Fig. S4). However, pathways for carbon fixation,
355 nitrogen and sulfur reduction, and oxidative phosphorylation were identified in a
356 relatively lower proportion relative to modules 3 and 6 (Fig. S4). Connectivity among
357 modules 4 and 5 was sparse in comparison to the large number of positive connections

358 among modules 1, 2, and 7. However, the overall functional potential was similar among

359 all five modules (1,2,4,5,7) (Fig. 4B, S4).

360

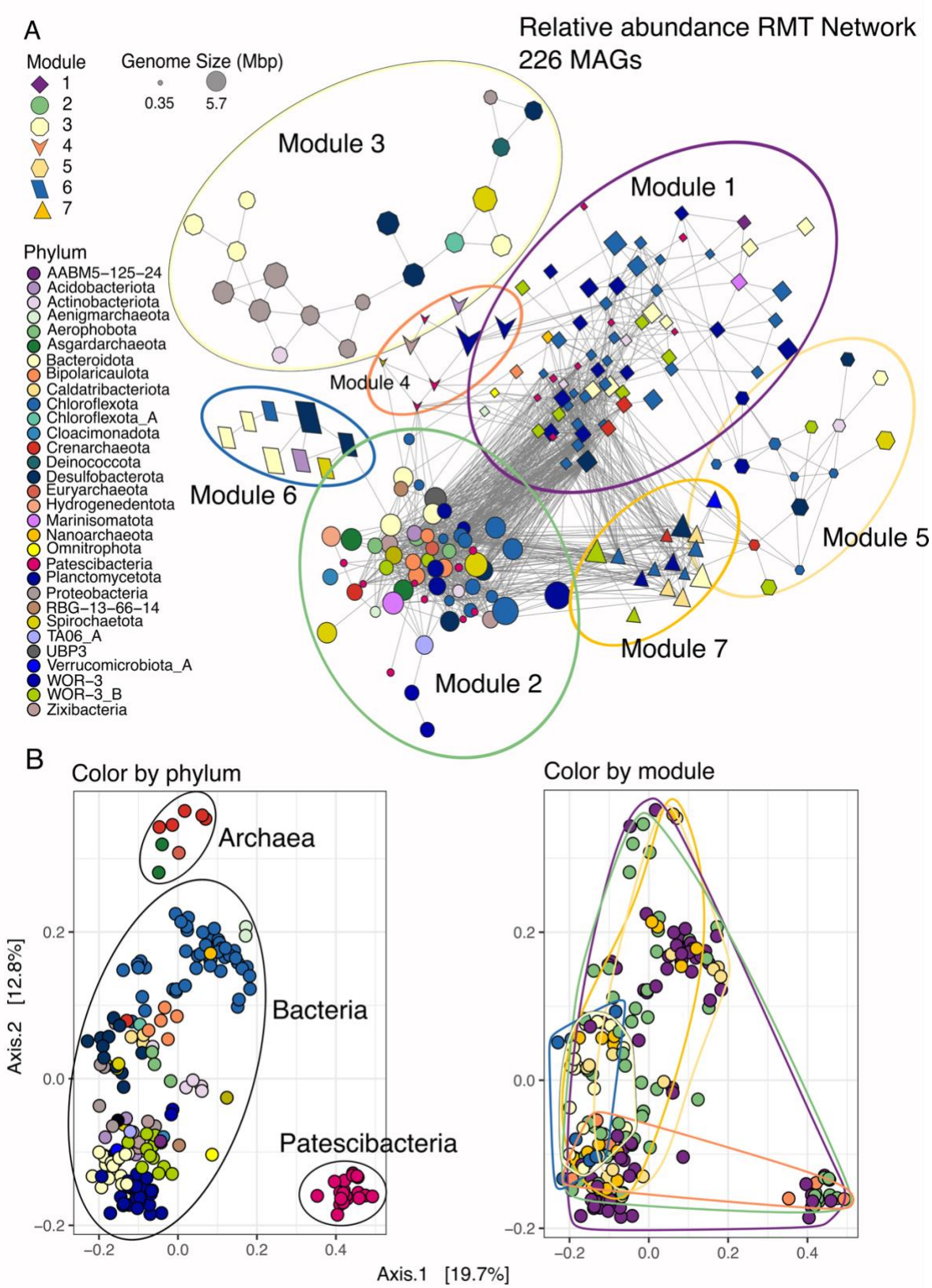
A
Relative abundance RMT Network
226 MAGs
Module
1
2
3
4
5
6
7
Genome Size (Mbp)
0.35
5.7
Phylum
AABM5−125−24
Acidobacteriota
Actinobacteriota
Aenigmarchaeota
Aerophobota
Asgardarchaeota
Bacteroidota
Bipolaricaulota
Caldatribacteriota
Chloroflexota
Chloroflexota_A
Cloacimonadota
Crenarchaeota
Deinococcota
Desulfobacterota
Euryarchaeota
Hydrogenedentota
Marinisomatota
Nanoarchaeota
Omnitrophota
Patescibacteria
Planctomycetota
Proteobacteria
RBG−13−66−14
Spirochaetota
TA06_A
UBP3
Verrucomicrobiota_A
WOR−3
WOR−3_B
Zixibacteria
Module 3
Module 1
Module 4
Module 6
Module 5
Module 7
Module 2
B
Color by phylum
Color by module
Archaea
Bacteria
Patescibacteria
Axis.2 [12.8%]
Axis.1 [19.7%]
0.2
0.0
−0.2
−0.2
0.0
0.2
0.4

361

362 Figure 4. A.) The random matrix theory derived co-occurrence network, based on MAG
363 relative abundance. The point size (genome size), color (phylum), and shape (module)
364 are used to describe each MAG in the network. All connections are significant and
365 positive. Ellipses are used to clarify the modules. B) The NMDS ordination of MAGs
366 included in the network based on KEGG functional potential. Both panels show the
367 same ordination, with the left panel colors indicating the phylum classification and right,
368 the module assignment. The key adjacent to panel A applies to the colors used for taxa
369 and modules shown in panel B.

370

371 *2.2 Modules containing widespread and abundant MAGs in sediment layers.*

372 The relative abundance of MAGs at the phylum level within a module was
373 consistent across sediment layers (Fig. 5). For example, the top four most abundant
374 phyla in module 1 included Chloroflexota, Planctomycetota, Bacteroidota, and
375 Actinobacteriota. In module 2, the cumulative relative abundance of Choloroflexota,
376 Planctomycetota, TA06, and WOR3-B were also among the most abundant phyla within
377 this module and were found in similar relative proportions in the sediment layers.

378 Despite the diversity of MAGs assigned to a particular phylum within a module, a
379 small number of MAGs were often the most abundant at all sediment depths. For
380 example, 12 of the 70 MAGs in module 1 represented the majority of reads recruited
381 (Fig. S5). The abundant MAGs in the module were distributed across 6 of the 13 phyla
382 in the module. Within module 1, 5 Chloroflexota MAGs were among the most abundant
383 (Fig. S5). Other phyla within the module were low diversity, such as TA06 in module 2,
384 where a single MAG was the sole contributor to the phylum level abundance patterns.

385 Although often detected in the entire depth profile, MAGs within modules 1, 2, 4
386 and 7 were especially abundant below 20 cm (Fig. 5, S4). Modules 1 and 2 contained
387 several Chloroflexota MAGs that collectively recruited at least 15% of the mapped

388 reads. Average coverage of these MAGs was over 50X in the majority of samples below
389 40 cm. Module 2 contained two of the most abundant MAGs below 40 cm, TA06 and
390 Bipolaricaulota, which recruited nearly 15% of mapped reads in many samples below
391 100 cm. The peak relative abundance of MAGs in modules 1, 2, 5, and 7 were distinct,
392 with module 1 peaking in abundance at 70-110 cm, module 2 peaking in all samples
393 below 100 cm, module 5 peaking at 30 - 40 cm, and module 7 peaking at 150 – 250 cm
394 (Fig S4).

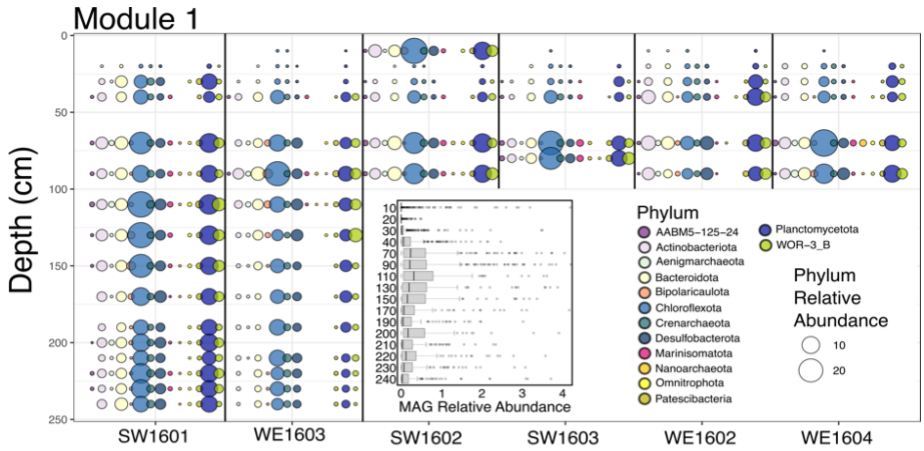
Module 1
Depth (cm)
MAG Relative Abundance
Phylum
AABM5-125-24
Actinobacteriota
Aenigmarchaeota
Bacteroidota
Bipolaricaulota
Chloroflexota
Crenarchaeota
Desulfobacterota
Marinisomatota
Nanoarchaeota
Omnitrophota
Patescibacteria
Planctomycetota
WOR-3_B
Phylum Relative Abundance
10
20
SW1601
WE1603
SW1602
SW1603
WE1602
WE1604

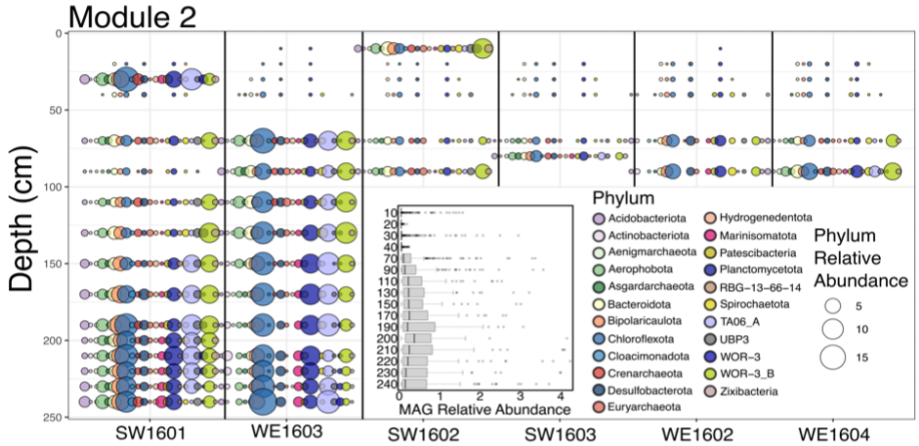
Module 2
Depth (cm)
MAG Relative Abundance
Phylum
Acidobacteriota
Actinobacteriota
Aenigmarchaeota
Aerophobota
Asgardarchaeota
Bacteroidota
Bipolaricaulota
Chloroflexota
Cloacimonadota
Crenarchaeota
Desulfobacterota
Euryarchaeota
Hydrogenedentota
Marinisomatota
Patescibacteria
Planctomycetota
RBG-13-66-14
Spirochaetota
TA06_A
UBP3
WOR-3
WOR-3_B
Zixibacteria
Phylum Relative Abundance
5
10
15
SW1601
WE1603
SW1602
SW1603
WE1602
WE1604

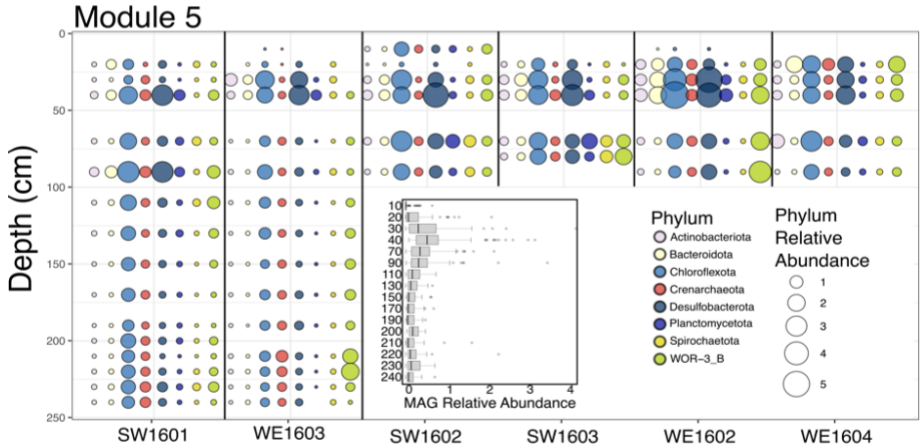
Module 5
Depth (cm)
MAG Relative Abundance
Phylum
Actinobacteriota
Bacteroidota
Chloroflexota
Crenarchaeota
Desulfobacterota
Planctomycetota
Spirochaetota
WOR-3_B
Phylum Relative Abundance
1
2
3
4
5
SW1601
WE1603
SW1602
SW1603
WE1602
WE1604

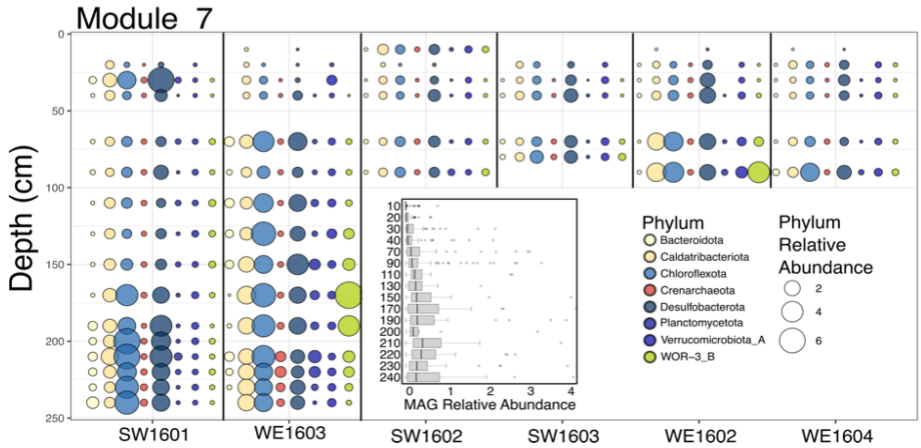
Module 7
Depth (cm)
MAG Relative Abundance
Phylum
Bacteroidota
Caldatribacteriota
Chloroflexota
Crenarchaeota
Desulfobacterota
Planctomycetota
Verrucomicrobiota_A
WOR-3_B
Phylum Relative Abundance
2
4
6
SW1601
WE1603
SW1602
SW1603
WE1602
WE1604

395

Figure 5. Bubble plots for the cumulative phylum level relative abundance of MAGs contained in each of the network modules. Relative abundance (size of the bubble) indicates the percentage of reads mapped to the MAGs glommed at the phylum level relative to the number of reads mapped to the sample. The colors for each phylum are congruent across all four panels. The box-whisker relative abundance plots nested within each box describe the relative abundance of MAGs in the module at each depth.

2.3 Unconnected MAGs are dominant in the upper 40 cm and potentially have a niche in the deepest sediment

In addition to MAGs that were associated with the modules described above, there were numerous unconnected MAGs that were predominantly located in sediments at or above 40 cm (Fig. S4). Proteobacteria (Pseudolabrys and Methyloceanibacter) and Crenarchaeota (Nitrososphaeraceae and Bathyarchaeia BA1) MAGs were among the most abundant unconnected MAGs. However, we also observed MAGs within many sediment layers that were abundant both in the upper 40 cm and below 200 cm within the core collected from West Creek (WE3) (Fig. S6). Although they maintained a patchy distribution in the surface, the relative abundance was consistent at 200-240 cm (Fig. S6). *Methyloceanibacter* MAGs identified in this “bimodal” group are putative bacterial methylotrophs (Vekeman et al. 2016), but none of the mags contained the methane monooxygenase or co-methyltransferase genes. Bimodal Nitrososphaeraceae MAGs contained ammonia oxidation potential (*amo*) and the *Pseudolabrys* contained sulfur oxidation (*sox*), sulfur reduction (*dsr, apr, sat*), and nitrate reduction potential (*narG*) (Fig. S6). These functions suggest a mix of aerobic and anaerobic respiration potential within the deepest layers sampled in the West creek sediment core.

421 *2.4 Bathyarchaeia BA1 are potentially important facilitators of abundant deep sediment*
422 *communities*

423 Because of the potentially important ecological role of Bathyarchaeia BA1 MAGs
424 in the network as connector hubs (Fig. S3) and global significance of this family to
425 carbon cycling (Hou et al. 2023), we focused on these MAGs and the connections to
426 other MAGs in the network to understand the potential relevance to carbon cycling. Our
427 network analysis identified 2 separate Bathyarchaeia BA1 MAGs that were connector
428 hubs in the RMT network (Fig. S3). To explore the potential role of these Bathyarchaeia
429 BA1 we created a subnetwork of MAGs that are directly connected to the Bathyarchaeia
430 MAGs, resulting in a total of 33 MAGs in the subnetwork (Fig 5A). Among the 12
431 different orders contained in the subnetwork were members of Bipolaricaulia, GIF9,
432 WOR3, Desulfatiglandales, and Caldatribacteriota and each of the four modules (1, 2, 5,
433 and 7) were represented (Fig. 6A). The relative abundance of members at the phylum
434 level in this subnetwork was also consistent across many of the samples (Fig. 6B).

435 **3. Putative functional complementarity among Bathyarchaeia subnetwork MAGs**
436 **suggests potential decomposition of hydrocarbon and aromatics**

437 *3.1 Consistent relative abundance among members of the Bathyarchaeia subnetwork*

438 Within the Bathyarchaeia subnetwork, GIF9 MAGs were the most abundant,
439 totaling 8 MAGs, all of which are putative acetogens based on their functional profile.
440 Six GIF9 MAGs were located in the same module (module 2), indicating a close
441 ecological connection and yet they were not identified as functionally redundant
442 members of the community according to the M2M analysis. The collective GIF9 MAG

443 relative abundance reached 15% in many of the samples below 20 cm, but like all
444 MAGs in the subnetwork, they were not excluded from the upper 20 cm (Fig. 6B).
445 Desulfatiglandales, Dehalococcoidales, and Planctomycetota were also among the
446 most abundant MAGs in the subnetwork and occurred at similar cumulative relative
447 abundances. The high correlation among these MAGs detected in the network is
448 reflected in the consistent relative abundance of the group members within a core and
449 generally across all six cores (Fig. 6B).

450

451 *3.2 Bathyarchaeia BA1 subnetwork MAGs use cooperative metabolism to degrade*
452 *aromatics*

453 M2M identified the putative functions of each community member and the added
454 value metabolites produced by minimal communities. An added value metabolite is one
455 produced through complementary metabolism among the microbes in a minimal
456 community, and a minimal community is defined as a cohort of MAGs required to
457 produce the entire set of metabolites in the collection of genomes. We found 82
458 metabolites that were producible by each of the 33 MAGs in the subnetwork (core
459 functions) and 1098 total metabolites could be produced by the individual organisms all
460 together (collective functions). The added value of cooperation within the minimal
461 communities required 22 bacteria and 20 essential symbionts to produce an additional
462 228 compounds. These 228 compounds were only possible when all members of a
463 minimal community had the potential to exchange metabolites. Redundant members of
464 the community that were identified in at least one, but not all minimal communities

465 included Dehalococcoidia – RBG-16-60-22, Caldatribacteriota JS1, Dehalococcoidia
466 AB-539-J10, and Dehalococcoidia UBA5760.

467 Among the 228 compounds that could be formed solely if organisms exchanged
468 compounds, key metabolites involved in anaerobic decomposition of aromatic
469 compounds were identified and the presence of the genes conferring capacity for these
470 putative functions were confirmed by METABOLIC. Benzoyl-CoA reductase (*bcr*) was
471 identified in the genomes of three Desulfatiglandales, a novel order of Cloroflexota, and
472 Bathyarchaeia. Genes to produce benzoyl-CoA from phenol (*ubiX*/*bsdC*) occurred in
473 two of the Desulfatiflandales, the Bathyarchaeia and Bacteroidales MAGs (Fig. 6C).
474 Phenylacetyl-CoA was also identified as a metabolite putatively produced through
475 functional complementarity within the subnetwork.

476

477 *3.3 Genomic potential for acetogenesis and metabolic versatility is common among the*
478 *Bathyarchaeia BA1 subnetwork*

479 Genes for heterotrophic and autotrophic acetogenesis, primarily through the
480 Wood-Ljungdahl (WL) pathway, were detected in 25 of the 33 genomes in the
481 Bathyarchaeia B26-1 subnetwork (Fig. 6C). These genes included acetyl-CoA
482 dehydrogenase (*acdA*), acetate kinase (*ack*), and phosphate acetyltransferase (*pta*).
483 *acdA* was the most commonly detected gene indicating acetogenic metabolism, and *acs*
484 (Acetyl-CoA synthetase) was commonly detected within the same MAG (Table S2). The
485 co-occurrence of genes encoding a putative WL pathway within most genomes and a
486 formate oxidation gene (*fae*) required to convert CO_2 into formate provides additional

487 evidence for synthesis of acetate from H_2 and CO_2. The genomic potential for the
488 production of acetate enabled by carbon fixation via the WL pathway was observed in
489 Desulfatiglandales, Bathyarchaeia, Dehalococcoidales, Chloroflexota, GIF9,
490 Bipolaricaulia, and Planctomycetota MAGs in the subnetwork (Fig. 6C). A WL pathway
491 was not detected in Caldatribacteriota, WOR3, and Bacteroidales. Instead, these MAGs
492 might produce acetate through fermentation of pyruvate or lactate. Most acetogens in
493 the network contain genes indicative of a flexible metabolic capacity through autotrophic
494 and/or fermentative acetate production (Fig. 6C).

495 We detected several additional pathways potentially related to energy
496 conservation among the members of the subnetwork. The presence of methane
497 monooxygenase regulatory protein (*mmoBD*) in Bipolaricaulia and Desulfatiglandales
498 (Fig. 6C) suggests methane oxidation potential. Additionally, aerobic carbon monoxide
499 dehydrogenase *coxSM* was detected in members of Bipolaricaulia, Caldatribacteriota,
500 Bathyarchaeia TCS64, and Desulfatiglandales. Additional pathways include selenate or
501 arsenate reduction potential in most of the subnetwork MAGs and one of the GIF9
502 MAGs contained genes for both pathways.

503

504

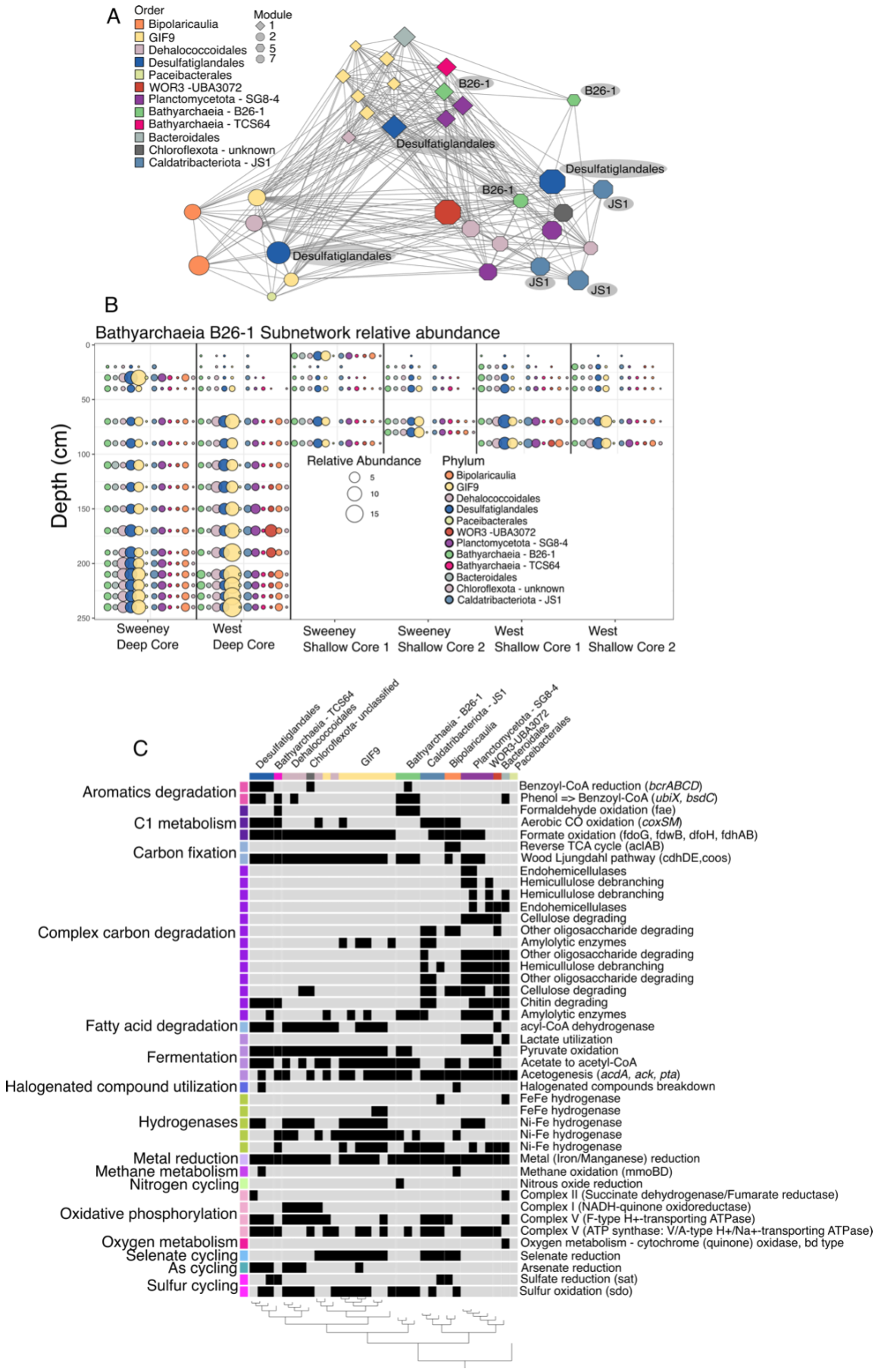
A
Order
Bipolaricaulia
GIF9
Dehalococcoidales
Desulfatiglandales
Paceibacterales
WOR3 -UBA3072
Planctomycetota - SG8-4
Bathyarchaeia - B26-1
Bathyarchaeia - TCS64
Bacteroidales
Chloroflexota - unknown
Caldatribacteriota - JS1
Module
1
2
5
7
B26-1
B26-1
Desulfatiglandales
Desulfatiglandales
B26-1
JS1
Desulfatiglandales
JS1
JS1
B
Bathyarchaeia B26-1 Subnetwork relative abundance
Depth (cm)
0
50
100
150
200
250
Relative Abundance
5
10
15
Phylum
Bipolaricaulia
GIF9
Dehalococcoidales
Desulfatiglandales
Paceibacterales
WOR3 -UBA3072
Planctomycetota - SG8-4
Bathyarchaeia - B26-1
Bathyarchaeia - TCS64
Bacteroidales
Chloroflexota - unknown
Caldatribacteriota - JS1
Sweeney Deep Core
West Deep Core
Sweeney Shallow Core 1
Sweeney Shallow Core 2
West Shallow Core 1
West Shallow Core 2
C
Desulfatiglandales
Bathyarchaeia - TCS64
Dehalococcoidales
Chloroflexota- unclassified
GIF9
Bathyarchaeia - B26-1
Caldatribacteriota - JS1
Bipolaricaulia
Planctomycetota - SG8-4
WOR3-UBA3072
Bacteroidales
Paceibacterales
Aromatics degradation
C1 metabolism
Carbon fixation
Complex carbon degradation
Fatty acid degradation
Fermentation
Halogenated compound utilization
Hydrogenases
Metal reduction
Methane metabolism
Nitrogen cycling
Oxidative phosphorylation
Oxygen metabolism
Selenate cycling
As cycling
Sulfur cycling
Benzoyl-CoA reduction (bcrABCD)
Phenol => Benzoyl-CoA (ubiX, bsdC)
Formaldehyde oxidation (fae)
Aerobic CO oxidation (coxSM)
Formate oxidation (fdoG, fdwB, dfoH, fdhAB)
Reverse TCA cycle (aclAB)
Wood Ljungdahl pathway (cdhDE,coos)
Endohemicellulases
Hemicullulose debranching
Hemicullulose debranching
Endohemicellulases
Cellulose degrading
Other oligosaccharide degrading
Amylolytic enzymes
Other oligosaccharide degrading
Hemicullulose debranching
Other oligosaccharide degrading
Cellulose degrading
Chitin degrading
Amylolytic enzymes
acyl-CoA dehydrogenase
Lactate utilization
Pyruvate oxidation
Acetate to acetyl-CoA
Acetogenesis (acdA, ack, pta)
Halogenated compounds breakdown
FeFe hydrogenase
FeFe hydrogenase
Ni-Fe hydrogenase
Ni-Fe hydrogenase
Ni-Fe hydrogenase
Metal (Iron/Manganese) reduction
Methane oxidation (mmoBD)
Nitrous oxide reduction
Complex II (Succinate dehydrogenase/Fumarate reductase)
Complex I (NADH-quinone oxidoreductase)
Complex V (F-type H+-transporting ATPase)
Complex V (ATP synthase: V/A-type H+/Na+-transporting ATPase)
Oxygen metabolism - cytochrome (quinone) oxidase, bd type
Selenate reduction
Arsenate reduction
Sulfate reduction (sat)
Sulfur oxidation (sdo)

505

506 Figure 6. A) The submodule of tightly correlated MAGs with connectivity among the four
507 subsurface modules. The shape in the network indicates module origin of each MAG,
508 the size represents the number of genes in the MAG, and the color is used for
509 taxonomic classification. Gray lines connecting the MAGs represent significant positive
510 correlations. B.) Bubble plot of relative abundance for MAG phylum level relative
511 abundance within the vertical profile of the sediment. The color of the bubble is based
512 on the phylum classification and matches the color in panel A. C) Select functional
513 annotation for all MAGs in the network. Functional potential of each MAG in the network
514 is described as presence (black bar) or absence (gray bar) for each function. Major
515 functional categories are shown on the left of the panel, and the taxonomic classification
516 of each MAG is shown at the top. MAGs are organized according to presence-absence
517 of the genes in the display and the hierarchical clustering tree is displayed at the bottom
518 of the panel.

519

520 Discussion

521 Salt marsh sediments contain diverse microbial communities with vast numbers
522 of uncultivated microbial organisms that are important to carbon storage and
523 biogeochemical cycling. Within the complex microbial communities inhabiting these
524 sediments, we identified metabolic complementarity important to cycling pools of
525 aromatic carbon among co-occurring groups of microbes. Bathyarchaeia BA1 was a key
526 member of each group of MAGs that were uniquely distributed within the sediment
527 profile, and they were primarily located below the dynamic upper layers of the sediment.
528 Another key finding was that similar genome populations exist throughout the entire
529 depth profile of multiple cores, spanning nearly 3000 years of sediment accumulation
530 (Bulseco 2018). This pattern may be the result of a burial process followed by
531 environmental selection and slow growth rates. Conversely, the upper layers of
532 sediment contain additional diverse MAGs with greater functional potential representing
533 the canonical pathways commonly associated with salt marsh microbial communities
534 (Baker et al. 2015; Tobias and Neubauer 2019). Our results are important for

535 understanding how the pools of organic carbon are shaped by microbial communities
536 within the less well characterized subsurface because we identify which microbes are
537 co-located, what forms of carbon may be made accessible due to metabolic
538 complementarity, and the underlying biogeochemical processes that preserve these
539 relationships.

540 **1. Potential metabolic flexibility is a key feature among MAGs in the zone of plant**
541 **and tidal influence.**

542 Plant roots and rhizomes along with bioturbating organism and other structural features
543 can increase permeability in the upper layers of the sediment (Guimond et al. 2020;
544 Moffett et al. 2012; Xiao et al. 2019) and these dynamic conditions potentially lead to
545 observed high diversity of microbial communities in the upper sediment layers. Redox
546 conditions and carbon availability can change rapidly in the upper sediment layers,
547 creating conditions where metabolic flexibility would be favored. As a result, there is a
548 decreased need for metabolic handoffs among members of the community.

549 Most of the MAGs that were unconnected in our network analysis were localized
550 in the dynamic upper layers of the sediment and did not occur below 90 cm. The
551 unconnected MAGs contained striking genomic versatility including the capacity to
552 utilize multiple electron acceptors for oxidation of diverse carbon sources, conduct
553 fermentation, and fix inorganic carbon. Many of the unconnected Proteobacteria and
554 Desulfobacterota MAGs contain the genomic potential for each of these metabolic
555 pathways in a single organism which was observed previously in similar sediments
556 (Vineis et al. 2023). This metabolic flexibility allows each of the members of the
557 community to inhabit a variety of conditions and this strategy makes sense given the

558 dynamic nature of these sediments. Members of these communities contain canonical
559 pathways that are commonly associated with carbon cycling in salt marsh sediments
560 including fermentation, denitrification, and sulfate reduction (Baker et al. 2015).

561 **2. Organic carbon decomposition in deeper sediment layers is potentially**
562 **facilitated by co-occurring community members with complimentary metabolic**
563 **pathways**

564 The consistency in relative abundance among members within the core
565 Bathyarchaeia subnetwork is a potential result of metabolic handoffs. Of particular
566 significance is the detection of benzoyl-CoA as a metabolite that could only be produced
567 by Bathyarchaeia, Dehalococcoidia, and Desulfatiglandales through metabolic handoffs
568 in the community. Benzoyl-CoA is a known intermediate involved in the anaerobic
569 decomposition of aromatic compounds toluene, phenol, ethylbenzene and benzoate
570 (Carmona et al. 2009; Porter and Young 2014). Under anaerobic conditions, reduction
571 of benzoyl-CoA leads to the production of acetyl-CoA which can enter into central
572 metabolic pathways for growth and energy conservation (Porter and Young 2014).
573 Phenylacetyl-CoA was also putatively produced through metabolic complementarity and
574 is similar to benzoyl-CoA, leading to the potential production acetyl-CoA/succinyl-CoA.
575 These metabolic pathways, central to aromatic decomposition are only possible due to
576 the potential metabolic handoffs among the subnetwork members. Although it is
577 possible that other combinations of MAGs could lead to the decomposition of aromatics,
578 co-occurrence provides additional support that handoffs among the genome populations
579 identified here are likely to occur in the environment.

580 Syntrophic interactions between a bacterial fermenter and CO_2 reduction are
581 often cited as important to the decomposition of aromatic carbon (Dai et al. 2024; Qiu et
582 al. 2006). The collective functional profile of the Bathyarchaeia subnetwork suggests
583 that the initial fermentation of complex organic carbon is conducted by members of the
584 Planctomycetota, WOR3, JS1 and others, followed by secondary decomposition of
585 aromatics by Bathyarchaeia, Deslufatiglandales, Chloroflexota. The products of
586 secondary fermentation, including H_2 and formate, usually used by methanogens, are
587 instead potentially being used by a diverse group of acetogens. Acetogens grow on
588 organic materials derived from cellulose, lignin, alcohols, hemicellulose, and chitin
589 within energy depleted sediments (Lever 2012; Yu et al. 2018), and there is evidence for
590 the use of lignin as an energy source in Bathyarchaeota (Yu et al. 2018).

591 These results suggest a central mechanism for carbon cycling among closely
592 coupled consortia within the sediment layers of salt marsh sediment. While this process
593 may be very slow, we have evidence from amplicon analysis of cDNA, that these
594 communities are active (Bulseco 2018). Conversion of these aromatics into microbial
595 biomass suggests that there may be a relevant cycling and/or recycling of carbon
596 stabilized by microbial activity even within these energy depleted sediments.

597 **3. Burial as a mechanism for aggregating putative consortia**

598 Burial as a mechanism for co-occurrence patterns has been suggested in energy
599 starved deep marine sediments where selection on the microbial community is thought
600 to result in low diversity (Kirkpatrick et al. 2019; Walsh et al. 2016). Previous studies of
601 microbial turnover within salt marshes described seasonal and transect community
602 compositional changes (Tebbe et al. 2022; Yao et al. 2019) or succession along a

603 chronosequence (Dini-Andreote et al. 2014; Wang et al. 2017). However, the
604 composition and stability of microbial communities within salt marsh sediments remains
605 relatively uncharacterized at the depths examine here.

606 Our study of the vertical sediment profile recovered two pieces of evidence that
607 suggests burial is a likely mechanism for the distribution of closely associated consortia.
608 The first observed pattern suggestive of burial was the recovery of MAGs assembled
609 independently from multiple depths in the same core that were dereplicated into a single
610 genome population. One of the strongest examples of this was observed in the
611 candidate phylum TA06, where a single population was recovered from 24 of the 55
612 samples, including every depth fraction except 10 cm. For dereplication to occur at this
613 scale (> 95% identity among MAGs in the dereplicated cluster), genome populations
614 would have experienced limited evolution over the nearly 3000 yrs of separation that
615 exists between the surface and bottom of the core. The second observed pattern was
616 the consistent relative abundance of MAGs within each module, relative to each other at
617 the phylum level (Fig. 5). The consistent relative abundance patterns among MAGs
618 within a module was observed both within the vertical sampling of an individual core and
619 across multiple cores. This is not to say that the relative abundance of members within
620 a module are the same at every depth across all cores. However, when the MAGs were
621 identified in a sample, they generally appear in similar ratios. The ratios of microbial
622 taxa might reflect the proportions required to support syntrophic interactions.

623 Similar compositions of sediment communities in marine systems have been
624 recovered from geographically distant communities (although at high taxonomic levels)
625 and were presumed to be subseafloor specialists (Inagaki et al. 2006; Petro et al. 2017;

2019). However, our data suggest that the same populations were buried within the sediment, essentially preserving the population through high selection coupled with slow growth.

The low porosity, small particle size, and low circulation observed in salt marsh sediments on the East Coast of the US (Guimond and Tamborski 2021) provide additional support to co-occurrence shaped by burial that we observed in our genomic data. The turnover of water within the sediment can require 30-90 years (Guimond and Tamborski 2021), depending on the marsh system, indicating that water flow from groundwater or surface sources may be limited. These physical characteristics present significant barriers to the dispersal of subsurface communities, leaving burial as a likely mechanism. One caveat to the low porosity and water flow are the observations in the deepest sediment layers collected from West Creek where we observed members of the community that require oxygen or terminal electron acceptors commonly associated with anaerobic shallow sediments. We speculate that the groundwater may potentially "well up" from below the bedrock or sand located beneath the salt marsh platform at this site.

Conclusion

The metabolic connections identified among correlated members of the microbial community provide key insights into how carbon is cycled by microbial communities within salt marsh sediments. Additionally, these results provide evidence for the mechanisms important to understanding the assembly and distribution of these communities. Our analysis identifies syntrophy among members of a putative core consortia that provides a potential mechanistic understanding of organic matter

decomposition. The process begins with decomposers of complex carbon, followed by aromatic decomposition, coupled with acetogenic energy conservation and finally oxidation of acetate through arsenate or selenate reduction. These findings represent a significant step forward in our understanding of how microbial communities survive within these energy limited systems and contribute to the stability of soil organic carbon in this blue carbon system. The persistent conversion of soil organic carbon by the microbial community indicates that the pools of carbon potentially originating from plant material undergo decomposition and transformation even under energy depleted conditions.

Data Availability

The data described here are described in the U.S. Department of Energy (DOE) Facilities Integrating Collaborations for User Science (FICUS) grant titled “Combining high resolution organic matter characterization and microbial meta-omics to assess the effects of nutrient loading on salt marsh carbon sequestration” (proposal ID = 503576, https://genome.jgi.doe.gov/portal/Comhiguestration/Comhiguestration.info.html). Supplemental data can be accessed using this link to a publicly available github page https://github.com/jvineis/DEEP-CORE-MANUSCRIPT.git

Acknowledgements

Samples were collected from the Plum Island Ecosystems LTER, which is supported by NSF (OCE 2224608) and from the NSF funded TIDE project (DEB

1902712). Sequencing was conducted at the Joint Genome Institute through a funded Facilities Integrating Collaborations for User Science (FICUS) grant (proposal ID 503576). Additional funding for this project was provided by an NSF PRFB to ANB (1907285), Simons Foundation (Grant #1247132 to ZGC, and Grant #01248016 to JLB), and Department of Energy (DOE DE-SC0024270).

References

Alneberg, Johannes, Brynjar Smári Bjarnason, Ino De Bruijn, et al. 2014. "Binning Metagenomic Contigs by Coverage and Composition." *Nature Methods* 11 (11): 1144–46. https://doi.org/10.1038/nmeth.3103.

Arndt, Sandra, B.B. Jørgensen, D.E. LaRowe, J.J. Middelburg, R.D. Pancost, and P. Regnier. 2013. "Quantifying the Degradation of Organic Matter in Marine Sediments: A Review and Synthesis." *Earth-Science Reviews* 123 (August): 53–86. https://doi.org/10.1016/j.earscirev.2013.02.008.

Baker, Brett J, Cassandre Sara Lazar, Andreas P Teske, and Gregory J Dick. 2015. "Genomic Resolution of Linkages in Carbon, Nitrogen, and Sulfur Cycling among Widespread Estuary Sediment Bacteria." *Microbiome* 3 (1): 14. https://doi.org/10.1186/s40168-015-0077-6.

Bankevich, Anton, Sergey Nurk, Dmitry Antipov, et al. 2012. "SPAdes: A New Genome Assembly Algorithm and Its Applications to Single-Cell Sequencing." *Journal of Computational Biology* 19 (5): 455–77. https://doi.org/10.1089/cmb.2012.0021.

Belcour, Arnaud, Clémence Frioux, Méziane Aite, Anthony Bretaudeau, Falk Hildebrand, and Anne Siegel. 2020. "Metage2Metabo, Microbiota-Scale Metabolic Complementarity for the Identification of Key Species." *eLife* 9 (December): e61968. https://doi.org/10.7554/eLife.61968.

Bulseco. 2018. "Nitrate as an Electron Acceptor in Microbial Decomposition of Salt Marsh Sediment Organic Matter and Implications for Carbon Storage." Northeastern University. https://doi.org/10.17760/D20293211.

Bulseco, Ashley N., Anne E. Giblin, Jane Tucker, et al. 2019. "Nitrate Addition Stimulates Microbial Decomposition of Organic Matter in Salt Marsh Sediments." *Global Change Biology* 25 (10): 3224–41. https://doi.org/10.1111/gcb.14726.

Bulseco, Ashley N., Joseph H. Vineis, Anna E. Murphy, et al. 2020. "Metagenomics Coupled with Biogeochemical Rates Measurements Provide Evidence That Nitrate Addition Stimulates Respiration in Salt Marsh Sediments." *Limnology and Oceanography* 65 (S1). https://doi.org/10.1002/lno.11326.

Campbell, Anthony D., Lola Fatoyinbo, Liza Goldberg, and David Lagomasino. 2022. "Global Hotspots of Salt Marsh Change and Carbon Emissions." *Nature* 612 (7941): 701–6. https://doi.org/10.1038/s41586-022-05355-z.

Capella-Gutiérrez, Salvador, José M. Silla-Martínez, and Toni Gabaldón. 2009. "trimAl: A Tool for Automated Alignment Trimming in Large-Scale Phylogenetic Analyses." *Bioinformatics* 25 (15): 1972–73. https://doi.org/10.1093/bioinformatics/btp348.

Carmona, Manuel, María Teresa Zamarro, Blas Blázquez, et al. 2009. "Anaerobic Catabolism of Aromatic Compounds: A Genetic and Genomic View." *Microbiology and Molecular Biology Reviews* 73 (1): 71–133. https://doi.org/10.1128/MMBR.00021-08.

Chaumeil, Pierre-Alain, Aaron J Mussig, Philip Hugenholtz, and Donovan H Parks. 2020. "GTDB-Tk: A Toolkit to Classify Genomes with the Genome Taxonomy Database." *Bioinformatics* 36 (6): 1925–27. https://doi.org/10.1093/bioinformatics/btz848.

Core Team, R. 2024. *R: A Language and Environment for Statistical Computing*. Released. https://www.R-project.org/.

Dai, Shixiang, Falk Harnisch, Micjel Chávez Morejón, Nina Sophie Keller, Benjamin Korth, and Carsten Vogt. 2024. "Microbial Electricity-Driven Anaerobic Phenol Degradation in Bioelectrochemical Systems." *Environmental Science and Ecotechnology* 17 (January): 100307. https://doi.org/10.1016/j.ese.2023.100307.

Deng, Ye, Yi-Huei Jiang, Yunfeng Yang, Zhili He, Feng Luo, and Jizhong Zhou. 2012. "Molecular Ecological Network Analyses." *BMC Bioinformatics* 13 (1): 113. https://doi.org/10.1186/1471-2105-13-113.

Dini-Andreote, Francisco, Michele De Cássia Pereira E Silva, Xavier Triadó-Margarit, Emilio O Casamayor, Jan Dirk Van Elsas, and Joana Falcão Salles. 2014. "Dynamics of Bacterial Community Succession in a Salt Marsh Chronosequence: Evidences for Temporal Niche Partitioning." *The ISME Journal* 8 (10): 1989–2001. https://doi.org/10.1038/ismej.2014.54.

Duarte, Carlos M., Iñigo J. Losada, Iris E. Hendriks, Inés Mazarrasa, and Núria Marbà. 2013. "The Role of Coastal Plant Communities for Climate Change Mitigation and Adaptation." *Nature Climate Change* 3 (11): 961–68. https://doi.org/10.1038/nclimate1970.

Erb, Hailey, Ashley Keiser, and Kristen M DeAngelis. 2024. "Salt Marsh Soil Organic Carbon Is Regulated by Drivers of Microbial Activity." *Sustainable Microbiology* 1 (1): qvae009. https://doi.org/10.1093/sumbio/qvae009.

Eren, A. Murat, Özcan C. Esen, Christopher Quince, et al. 2015. "Anvi'o: An Advanced Analysis and Visualization Platform for 'omics Data." *PeerJ* 3: e1319.

Eren, A. Murat, Evan Kiefl, Alon Shaiber, et al. 2020. “Community-Led, Integrated, Reproducible Multi-Omics with Anvi’o.” *Nature Microbiology* 6 (1): 3–6. https://doi.org/10.1038/s41564-020-00834-3.

Feng, Kai, Xi Peng, Zheng Zhang, et al. 2022. “iNAP: An Integrated Network Analysis Pipeline for Microbiome Studies.” *iMeta* 1 (2): e13. https://doi.org/10.1002/imt2.13.

Fontaine, Sébastien, Sébastien Barot, Pierre Barré, Nadia Bdioui, Bruno Mary, and Cornelia Rumpel. 2007. “Stability of Organic Carbon in Deep Soil Layers Controlled by Fresh Carbon Supply.” *Nature* 450 (7167): 277–80. https://doi.org/10.1038/nature06275.

Frioux, Clémence, Enora Fremy, Camille Trottier, and Anne Siegel. 2018. “Scalable and Exhaustive Screening of Metabolic Functions Carried out by Microbial Consortia.” *Bioinformatics* 34 (17): i934–43. https://doi.org/10.1093/bioinformatics/bty588.

Gallagher, John L., and F. Gerald Plumley. 1979. “Underground Biomass Profiles and Productivity in Atlantic Coastal Marshes.” *American Journal of Botany* 66 (2): 156–61. https://doi.org/10.1002/j.1537-2197.1979.tb06208.x.

Gibson, Scott M., Stephen P. Ficklin, Sven Isaacson, Feng Luo, Frank A. Feltus, and Melissa C. Smith. 2013. “Massive-Scale Gene Co-Expression Network Construction and Robustness Testing Using Random Matrix Theory.” *PLoS ONE* 8 (2): e55871. https://doi.org/10.1371/journal.pone.0055871.

Guimond, Julia A, Angelia L Seyfferth, Kevan B Moffett, and Holly A Michael. 2020. “A Physical-Biogeochemical Mechanism for Negative Feedback between Marsh Crabs and Carbon Storage.” *Environmental Research Letters* 15 (3): 034024. https://doi.org/10.1088/1748-9326/ab60e2.

Guimond, Julia A, and Joseph Tamborski. 2021. “Salt Marsh Hydrogeology: A Review.” *Water* 13 (4): 543. https://doi.org/10.3390/w13040543.

Howes, Brian L., John W. H. Dacey, and Gary M. King. 1984. “Carbon Flow through Oxygen and Sulfate Reduction Pathways in Salt Marsh Sediments1.” *Limnology and Oceanography* 29 (5): 1037–51. https://doi.org/10.4319/lo.1984.29.5.1037.

Inagaki, Fumio, Takuro Nunoura, Satoshi Nakagawa, et al. 2006. “Biogeographical Distribution and Diversity of Microbes in Methane Hydrate-Bearing Deep Marine Sediments on the Pacific Ocean Margin.” *Proceedings of the National Academy of Sciences* 103 (8): 2815–20. https://doi.org/10.1073/pnas.0511033103.

Jain, Chirag, Luis M. Rodriguez-R, Adam M. Phillippy, Konstantinos T. Konstantinidis, and Srinivas Aluru. 2018. “High Throughput ANI Analysis of 90K Prokaryotic Genomes Reveals Clear Species Boundaries.” *Nature Communications* 9 (1): 5114. https://doi.org/10.1038/s41467-018-07641-9.

Jørgensen, Bo Barker, and Antje Boetius. 2007. “Feast and Famine — Microbial Life in the Deep-Sea Bed.” *Nature Reviews Microbiology* 5 (10): 770–81. https://doi.org/10.1038/nrmicro1745.

Kirkpatrick, John B., Emily A. Walsh, and Steven D’Hondt. 2019. “Microbial Selection and Survival in Subseafloor Sediment.” *Frontiers in Microbiology* 10 (May): 956. https://doi.org/10.3389/fmicb.2019.00956.

Kirwan, Matthew L., J. Patrick Megonigal, Genevieve L. Noyce, and Alexander J. Smith. 2023. “Geomorphic and Ecological Constraints on the Coastal Carbon Sink.” *Nature Reviews Earth & Environment* 4 (6): 393–406. https://doi.org/10.1038/s43017-023-00429-6.

Kuzyakov, Yakov, and Evgenia Blagodatskaya. 2015. “Microbial Hotspots and Hot Moments in Soil: Concept & Review.” *Soil Biology and Biochemistry* 83 (April): 184–99. https://doi.org/10.1016/j.soilbio.2015.01.025.

Langmead, Ben, and Steven L Salzberg. 2012. “Fast Gapped-Read Alignment with Bowtie 2.” *Nature Methods* 9 (4): 357–59. https://doi.org/10.1038/nmeth.1923.

Lever, Mark Alexander. 2012. “Acetogenesis in the Energy-Starved Deep Biosphere – A Paradox?” *Frontiers in Microbiology* 2. https://doi.org/10.3389/fmicb.2011.00284.

Li, Heng, Bob Handsaker, Alec Wysoker, et al. 2009. “The Sequence Alignment/Map Format and SAMtools.” *Bioinformatics* 25 (16): 2078–79. https://doi.org/10.1093/bioinformatics/btp352.

Liang, Chao, Joshua P. Schimel, and Julie D. Jastrow. 2017. “The Importance of Anabolism in Microbial Control over Soil Carbon Storage.” *Nature Microbiology* 2 (8): 17105. https://doi.org/10.1038/nmicrobiol.2017.105.

Liu, Jin-e, Rui-Ming Han, Hai-Rong Su, et al. 2017. “Effects of Exotic Spartina Alterniflora on Vertical Soil Organic Carbon Distribution and Storage Amount in Coastal Salt Marshes in Jiangsu, China.” *Ecological Engineering* 106 (September): 132–39. https://doi.org/10.1016/j.ecoleng.2017.05.041.

Luo, Feng, Yunfeng Yang, Jianxin Zhong, et al. 2007. “Constructing Gene Co-Expression Networks and Predicting Functions of Unknown Genes by Random Matrix Theory.” *BMC Bioinformatics* 8 (1): 299. https://doi.org/10.1186/1471-2105-8-299.

Mcleod, Elizabeth, Gail L Chmura, Steven Bouillon, et al. 2011. “A Blueprint for Blue Carbon: Toward an Improved Understanding of the Role of Vegetated Coastal Habitats in Sequestering CO_2.” *Frontiers in Ecology and the Environment* 9 (10): 552–60. https://doi.org/10.1890/110004.

Moffett, Kevan B., Steven M. Gorelick, Robert G. McLaren, and Edward A. Sudicky. 2012. “Salt Marsh Ecohydrological Zonation Due to Heterogeneous Vegetation–

Groundwater–Surface Water Interactions." *Water Resources Research* 48 (2): 2011WR010874. https://doi.org/10.1029/2011WR010874.

Newman, M. E. J. 2004. "Fast Algorithm for Detecting Community Structure in Networks." *Physical Review E* 69 (6): 066133. https://doi.org/10.1103/PhysRevE.69.066133.

Oksanen, Jari, Gavin Simpson, Guillaume Blanchet, et al. 2024. *Vegan: Community Ecology Package*. Version 2.6-10. Released. https://CRAN.R-project.org/package=vegan.

Olesen, Jens M., Jordi Bascompte, Yoko L. Dupont, and Pedro Jordano. 2006. "The Smallest of All Worlds: Pollination Networks." *Journal of Theoretical Biology* 240 (2): 270–76. https://doi.org/10.1016/j.jtbi.2005.09.014.

Olm, Matthew R, Christopher T Brown, Brandon Brooks, and Jillian F Banfield. 2017. "dRep: A Tool for Fast and Accurate Genomic Comparisons That Enables Improved Genome Recovery from Metagenomes through de-Replication." *The ISME Journal* 11 (12): 2864–68. https://doi.org/10.1038/ismej.2017.126.

Ouyang, X., and S. Y. Lee. 2014. "Updated Estimates of Carbon Accumulation Rates in Coastal Marsh Sediments." *Biogeosciences* 11 (18): 5057–71. https://doi.org/10.5194/bg-11-5057-2014.

Parks, Donovan H., Michael Imelfort, Connor T. Skennerton, Philip Hugenholtz, and Gene W. Tyson. 2015. "CheckM: Assessing the Quality of Microbial Genomes Recovered from Isolates, Single Cells, and Metagenomes." *Genome Research* 25 (7): 1043–55. https://doi.org/10.1101/gr.186072.114.

Payne, Paige E., Loren N. Knobbe, Patricia Chanton, Julian Zaugg, Behzad Mortazavi, and Olivia U. Mason. 2025. "Uncovering Novel Functions of the Enigmatic, Abundant, and Active *Anaerolineae* in a Salt Marsh Ecosystem." *mSystems* 10 (1): e01162-24. https://doi.org/10.1128/msystems.01162-24.

Peng, Qiannan, Lu Lin, Qichao Tu, et al. 2023. "Unraveling the Roles of Coastal Bacterial Consortia in Degradation of Various Lignocellulosic Substrates." *mSystems*, July 7, e01283-22. https://doi.org/10.1128/msystems.01283-22.

Petro, Caitlin, Piotr Starnawski, Andreas Schramm, and Kasper U. Kjeldsen. 2017. "Microbial Community Assembly in Marine Sediments." *Aquatic Microbial Ecology* 79 (3): 177–95. https://doi.org/10.3354/ame01826.

Petro, Caitlin, Birthe Zäncker, Piotr Starnawski, et al. 2019. "Marine Deep Biosphere Microbial Communities Assemble in Near-Surface Sediments in Aarhus Bay." *Frontiers in Microbiology* 10 (April): 758. https://doi.org/10.3389/fmicb.2019.00758.

Porter, Abigail W., and Lily Y. Young. 2014. “Benzoyl-CoA, a Universal Biomarker for Anaerobic Degradation of Aromatic Compounds.” In *Advances in Applied Microbiology*, vol. 88. Elsevier. https://doi.org/10.1016/B978-0-12-800260-5.00005-X.

Price, M. N., P. S. Dehal, and A. P. Arkin. 2009. “FastTree: Computing Large Minimum Evolution Trees with Profiles Instead of a Distance Matrix.” *Molecular Biology and Evolution* 26 (7): 1641–50. https://doi.org/10.1093/molbev/msp077.

Qiu, Yan-Ling, Yuji Sekiguchi, Satoshi Hanada, et al. 2006. “Pelotomaculum Terephthalicum Sp. Nov. and Pelotomaculum Isophthalicum Sp. Nov.: Two Anaerobic Bacteria That Degrade Phthalate Isomers in Syntrophic Association with Hydrogenotrophic Methanogens.” *Archives of Microbiology* 185 (3): 172–82. https://doi.org/10.1007/s00203-005-0081-5.

Seitz, Kiley W, Cassandre S Lazar, Kai-Uwe Hinrichs, Andreas P Teske, and Brett J Baker. 2016. “Genomic Reconstruction of a Novel, Deeply Branched Sediment Archaeal Phylum with Pathways for Acetogenesis and Sulfur Reduction.” *The ISME Journal* 10 (7): 1696–705. https://doi.org/10.1038/ismej.2015.233.

Shannon, Paul, Andrew Markiel, Owen Ozier, et al. 2003. “Cytoscape: A Software Environment for Integrated Models of Biomolecular Interaction Networks.” *Genome Research* 13 (11): 2498–504. https://doi.org/10.1101/gr.1239303.

Spivak, Amanda C., Jonathan Sanderman, Jennifer L. Bowen, Elizabeth A. Canuel, and Charles S. Hopkinson. 2019. “Global-Change Controls on Soil-Carbon Accumulation and Loss in Coastal Vegetated Ecosystems.” *Nature Geoscience* 12 (9): 685–92. https://doi.org/10.1038/s41561-019-0435-2.

Stewart, Robert D., Marc D. Auffret, Amanda Warr, et al. 2018. “Assembly of 913 Microbial Genomes from Metagenomic Sequencing of the Cow Rumen.” *Nature Communications* 9 (1): 870. https://doi.org/10.1038/s41467-018-03317-6.

Tebbe, Dennis Alexander, Simone Geihser, Bernd Wemheuer, Rolf Daniel, Hendrik Schäfer, and Bert Engelen. 2022. “Seasonal and Zonal Succession of Bacterial Communities in North Sea Salt Marsh Sediments.” *Microorganisms* 10 (5): 859. https://doi.org/10.3390/microorganisms10050859.

Tobias, Craig, and Scott C. Neubauer. 2019. “Salt Marsh Biogeochemistry—An Overview.” In *Coastal Wetlands*. Elsevier. https://doi.org/10.1016/B978-0-444-63893-9.00016-2.

Vineis, Joseph H, Ashley N Bulseco, and Jennifer L Bowen. 2023. “Microbial Chemolithoautotrophs Are Abundant in Salt Marsh Sediment Following Long-Term Experimental Nitrate Enrichment.” *FEMS Microbiology Letters* 370 (January): fnad082. https://doi.org/10.1093/femsle/fnad082.

Walsh, Emily A, John B Kirkpatrick, Scott D Rutherford, David C Smith, Mitchell Sogin, and Steven D'Hondt. 2016. "Bacterial Diversity and Community Composition from Seasurface to Subseafloor." *The ISME Journal* 10 (4): 979–89. https://doi.org/10.1038/ismej.2015.175.

Wang, Miao, Erqin Li, Chen Liu, Alexandre Jousset, and Joana F. Salles. 2017. "Functionality of Root-Associated Bacteria along a Salt Marsh Primary Succession." *Frontiers in Microbiology* 8 (October): 2102. https://doi.org/10.3389/fmicb.2017.02102.

Xiao, Kai, Alicia M. Wilson, Hailong Li, and Carolyn Ryan. 2019. "Crab Burrows as Preferential Flow Conduits for Groundwater Flow and Transport in Salt Marshes: A Modeling Study." *Advances in Water Resources* 132 (October): 103408. https://doi.org/10.1016/j.advwatres.2019.103408.

Yao, Zhiyuan, Shicong Du, Chunling Liang, et al. 2019. "Bacterial Community Assembly in a Typical Estuarine Marsh with Multiple Environmental Gradients." *Applied and Environmental Microbiology* 85 (6): e02602-18. https://doi.org/10.1128/AEM.02602-18.

Yu, Tiantian, Weichao Wu, Wenyue Liang, Mark Alexander Lever, Kai-Uwe Hinrichs, and Fengping Wang. 2018. "Growth of Sedimentary Bathyarchaeota on Lignin as an Energy Source." *Proceedings of the National Academy of Sciences* 115 (23): 6022–27. https://doi.org/10.1073/pnas.1718854115.

Zhou, Zhichao, Patricia Q. Tran, Adam M. Breister, et al. 2022. "METABOLIC: High-Throughput Profiling of Microbial Genomes for Functional Traits, Metabolism, Biogeochemistry, and Community-Scale Functional Networks." *Microbiome* 10 (1): 33. https://doi.org/10.1186/s40168-021-01213-8.

Zimmermann, Johannes, Christoph Kaleta, and Silvio Waschina. 2021. "Gapseq: Informed Prediction of Bacterial Metabolic Pathways and Reconstruction of Accurate Metabolic Models." *Genome Biology* 22 (1): 81. https://doi.org/10.1186/s13059-021-02295-1.